

Probing Reionization-Era Galaxies with JWST UV Luminosity Functions and Large-Scale Clustering

Anirban Chakraborty¹ and Tirthankar Roy Choudhury

National Centre for Radio Astrophysics, Tata Institute of Fundamental Research,
Pune University Campus, Ganeshkhind, Pune 411007, India.

E-mail: anirban@ncra.tifr.res.in; anirban.chakraborty096@gmail.com;
tirth@ncra.tifr.res.in

Abstract. The James Webb Space Telescope (JWST) has transformed our understanding of early galaxy formation, providing an unprecedented view of the first billion years of cosmic history. These observations offer a crucial opportunity to probe the interplay between galaxy formation and reionization, placing stringent constraints on theoretical models. In this work, we build upon our previously developed semi-analytical framework that self-consistently models the evolving UV luminosity function (UVLF) of galaxies and the global reionization history while incorporating the effects of radiative feedback. Comparing our predictions with JWST and HST data, we identify a fundamental tension: models that match the UVLF fail to reproduce the observed evolution of galaxy clustering (bias) with redshift, and vice versa. To resolve this, we introduce a mass-dependent duty cycle linked to star formation duration. This duty cycle approaches unity at $z > 11$, requiring either enhanced UV radiation production or increased star formation efficiency to match the JWST UVLFs, while declining towards lower redshifts ($5 < z \leq 9$) to remain consistent with the bias measurements. Reconciling theory with observations requires that the characteristic star formation timescale increases from ≈ 80 Myr at $z \approx 6$ to ≈ 120 Myr at $z \approx 8$. Finally, our extended model, assuming a halo mass-independent escape fraction of $\approx 12\%$, produces a reionization history consistent with current constraints. These findings underscore the importance of jointly constraining high-redshift galaxy models using both UVLF and bias statistics to accurately interpret JWST data and refine our understanding of early cosmic evolution.

Keywords: high redshift galaxies, semi-analytic modeling, reionization

ArXiv ePrint: —

¹Corresponding author.

Contents

1	Introduction	1
2	Theoretical Formalism: The Baseline Model	2
3	Observational Datasets and Likelihood Analysis	5
4	Results from the baseline model	7
5	Extensions to the baseline model: Inclusion of duty cycle	12
6	Conclusion	19

1 Introduction

Understanding the formation and evolution of galaxies in the early Universe is one of the most fundamental areas of research in modern cosmology. In the hierarchical model of structure formation, dark matter halos serve as the cradles where galaxies form and evolve. As a result, the statistical and physical properties of galaxies are expected to be closely tied to those of their parent dark matter halos. Unraveling this relationship, commonly referred to as the ‘galaxy-halo connection’, can offer critical insights into the astrophysical processes that govern star formation within dark matter halos (see [1] for a review).

Over the past decade, the ultraviolet luminosity function (UVLF) has emerged as an important observable for understanding the statistical properties of galaxies. Deep imaging surveys with space- and ground-based facilities, such as the Subaru Telescope, Hubble Space Telescope (HST), and more recently, James Webb Space Telescopes (JWST), have enabled measurements of UVLFs at high redshifts ($z \geq 6$) and even out to redshifts as high as $z \approx 14$ [2–13]. These measurements have been widely used to understand how high redshift galaxies populate dark matter halos [14–22]. However, one-point statistics such as the UVLFs would have been sufficient for constraining the galaxy-halo connection at high redshifts if the mapping between the observed light from galaxies and their host dark-matter halo properties were strictly one-to-one. Instead, the complex interplay of different baryonic processes within dark matter halos gives rise to a complex relationship between galaxy properties and their host halos, allowing for multiple ways to populate galaxies inside dark matter halos while still producing the same number density of galaxies as a function of luminosity [23–27]. Therefore, to distinguish between widely different models of galaxy-halo connection, that are otherwise tuned to reproduce the observed UVLFs, one needs to consider other higher-order summary statistics of galaxies. In this regard, measuring the clustering of galaxies detected in large-scale surveys can prove to be very useful [25, 28–31]. An important quantity obtained from these two-point correlation studies is the galaxy bias, which quantifies the extra clustering of galaxies compared to the underlying dark matter distribution in the Universe. Since the clustering strength of dark matter halos is known to depend on their mass [32–35], measurements of the galaxy bias provide a means to infer the masses of the halos hosting these galaxies, thereby placing tighter constraints on how high- z galaxies populate dark matter halos [36–38].

While clustering studies have been widely conducted at lower redshifts to investigate the host halo properties of Lyman-break galaxies, e.g., [36, 39, 40], such analyses at higher redshifts have been considerably more challenging due to the lack of a statistical sample of high- z galaxies, with only a handful of studies available for $z > 6$ [7, 37, 41–43]. However, exploiting the increased depth, sensitivity, and wide-field coverage of the instruments onboard JWST, it has recently been possible to measure the angular clustering of galaxies during the first billion years of the Universe, out to redshifts of $z \approx 11$ [44]. Therefore, it is essential to check whether the wide variety of galaxy-halo connection models, that had been proposed to explain the overabundance of UV-bright galaxies [9, 21, 26, 45–51] seen in JWST observations, remain consistent with these latest observations of galaxy two-point statistics. In this paper, our primary goal is, therefore, to obtain insights into the astrophysical properties of high-redshift galaxies by comparing the self-consistently coupled theoretical model of high- z galaxy formation, evolution, and cosmic reionization, introduced in our previous work [50] (hereafter, CC24), against the most recent and updated JWST UVLF and clustering measurements as well as constraints on the progress of reionization. In this work, the cosmological parameters are taken to be $\Omega_m = 0.308$, $\Omega_\Lambda = 0.692$, $\Omega_b = 0.0482$, $h = 0.678$, $\sigma_8 = 0.829$ and $n_s = 0.961$ [52].

The paper is organized as follows: In Section 2, we describe the details of the theoretical model from our previous work (CC24). Section 3 describes the various observational datasets used in this work and the Bayesian formalism used for parameter estimation. We discuss the results obtained from comparing our earlier model to the observational datasets presently available in Section 4. In Section 5, we discuss some modifications to this model that can help in explaining all the different observables simultaneously. Finally, we conclude with a summary of our main results in Section 6.

2 Theoretical Formalism: The Baseline Model

In this section, we describe the theoretical framework for modelling the star formation and ionizing properties of galaxies at high redshifts and calculating the different global high-redshift galaxy and reionization observables.

In CC24, we presented a semi-analytical framework for modeling the astrophysical properties of high-redshift galaxies. This model calculates the evolving galaxy UV luminosity function across a wide range of redshifts and simultaneously tracks the evolution of the neutral hydrogen fraction in the intergalactic medium with time. While computing various galaxy observables, it self-consistently accounts for the effects of reionization feedback, which suppresses star formation in low-mass galaxies. We briefly summarize here the main features of the model and refer interested readers to CC24 for more details. We will refer to this model as the **baseline** model.

In this model, each dark matter halo is assumed to host only one galaxy, whose properties are primarily determined by the mass of the halo that hosts it. For instance, the star-formation rate \dot{M}_* of a galaxy residing within a halo of mass M_h is calculated as

$$\dot{M}_*(M_h, z) = \frac{M_*(M_h, z)}{t_*(z)} = \frac{f_*(M_h, z)}{c_* t_H(z)} f_{\text{gas}}(M_h) \left(\frac{\Omega_b}{\Omega_m} \right) M_h, \quad (2.1)$$

In the equation above, $f_*(M_h, z)$ denotes the star-formation efficiency (i.e., the fraction of baryons within halos that are converted into stars), $f_{\text{gas}}(M_h)$ represents the gas fraction retained inside a halo after photoheating due to the rising ionizing UV background, and

$t_*(z) = c_* t_H(z)$ is the average star formation time scale, where $t_H(z) = H^{-1}(z)$ is the local Hubble time. For feedback-affected halos, the gas fraction is assumed to be $f_{\text{gas}}(M_h) = 2^{-M_{\text{crit}}/M_h}$, wherein the parameter M_{crit} represents the characteristic mass of halos which are capable of retaining 50 percent of their gas reservoir. We set $f_{\text{gas}}(M_h)$ to be unity for halos located in neutral regions, where radiative feedback is absent.

As a result, the monochromatic rest-frame UV luminosity (L_{UV}), which is calculated from the star-formation rate (SFR) using a constant conversion factor \mathcal{K}_{UV} ¹, depends on the extent to which a galaxy is affected by radiative feedback due to reionization. The UV luminosity of a galaxy hosted by a halo of mass M_h is given by the following relations -

$$L_{\text{UV}}^{\text{nofb}} = \frac{1}{\mathcal{K}_{\text{UV}}} \frac{M_*(M_h, z)}{t_*(z)} = \frac{1}{\mathcal{K}_{\text{UV, fid}}} \frac{\varepsilon_{*10, \text{UV}}(z)}{t_H(z)} \left(\frac{M_h}{10^{10} M_\odot} \right)^{\alpha_*(z)} \left(\frac{\Omega_b}{\Omega_m} \right) M_h \quad (2.2)$$

and,

$$L_{\text{UV}}^{\text{fb}} = 2^{-M_{\text{crit}}/M_h} L_{\text{UV}}^{\text{nofb}} \quad (2.3)$$

where, the superscripts “nofb” and “fb” denote that the corresponding relation applies to galaxies in the absence and presence of radiative feedback, respectively. These $M_h - L_{\text{UV}}$ relations assume that the star-formation efficiency is parameterised as $f_*(M_h, z) = f_{*,10}(z) (M_h/10^{10} M_\odot)^{\alpha_*(z)}$. Furthermore, the “UV efficiency” parameter $\varepsilon_{*10, \text{UV}}$ appearing in equations (2.2) and (2.3) is a combination of several other parameters introduced earlier and is defined as,

$$\varepsilon_{*10, \text{UV}} \equiv \frac{f_{*,10}}{c_*} \frac{\mathcal{K}_{\text{UV, fid}}}{\mathcal{K}_{\text{UV}}}. \quad (2.4)$$

The rest-frame UV luminosities obtained from this model are finally converted to absolute UV magnitude (in the AB system) using the relation [53, 54] -

$$\log_{10} \left(\frac{L_{\text{UV}}}{\text{ergs s}^{-1} \text{ Hz}^{-1}} \right) = 0.4 \times (51.6 - M_{\text{UV}}). \quad (2.5)$$

At a given redshift z , the globally averaged UV luminosity function ($\Phi_{\text{UV}}^{\text{total}}$) is thereafter obtained by appropriately combining the feedback-affected UV luminosity function ($\Phi_{\text{UV}}^{\text{fb}}$) from ionized regions and the feedback-unaffected UV luminosity function ($\Phi_{\text{UV}}^{\text{nofb}}$) from neutral regions.

$$\begin{aligned} \Phi_{\text{UV}}^{\text{total}}(z) &= Q_{\text{HII}}(z) \Phi_{\text{UV}}^{\text{fb}} + [1 - Q_{\text{HII}}(z)] \Phi_{\text{UV}}^{\text{nofb}} \\ &= Q_{\text{HII}}(z) \frac{dn}{dM_h} \left| \frac{dM_h}{dL_{\text{UV}}^{\text{fb}}} \right| \left| \frac{dL_{\text{UV}}^{\text{fb}}}{dM_{\text{UV}}} \right| + [1 - Q_{\text{HII}}(z)] \frac{dn}{dM_h} \left| \frac{dM_h}{dL_{\text{UV}}^{\text{nofb}}} \right| \left| \frac{dL_{\text{UV}}^{\text{nofb}}}{dM_{\text{UV}}} \right|, \end{aligned} \quad (2.6)$$

where $Q_{\text{HII}}(z)$ is the globally averaged ionization fraction at redshift z and dn/dM_h is dark matter halo mass function. We adopt the fitting formula from Jenkins et al. (2001) [34] for dn/dM_h .

We self-consistently compute the globally averaged ionization fraction Q_{HII} , which is required for determining the UVLF (see equation (2.6)), from the model assuming star-forming galaxies to be the only sources of ionizing photons at high redshifts. This calculation requires information about the intrinsic ionizing photon production rate per unit comoving

¹This conversion factor \mathcal{K}_{UV} is defined as $L_{\text{UV}} = \dot{M}_*(M_h, z)/\mathcal{K}_{\text{UV}}$ and depends on the star formation history as well as the assumed properties of the stellar population (age, IMF, binarity, metallicity).

volume within a galaxy as well as the fraction of these photons that escape the galaxy and reach the IGM. We model the intrinsic photon production rate in a halo in terms of its star formation rate and the number of ionizing photons emitted per unit mass of stars formed ($\eta_{\gamma*}$). We further assume the escape fraction of hydrogen ionizing photons to have a power-law dependence on the host DM halo mass, given by $f_{\text{esc}}(M_h) = f_{\text{esc},10}(M_h/10^{10}M_\odot)^{\alpha_{\text{esc}}}$. Under these assumptions, the number density of ionizing photons per unit comoving volume contributed by feedback-affected galaxies, $\dot{n}_{\text{ion}}^{\text{fb}}(z)$, is calculated as

$$\dot{n}_{\text{ion}}^{\text{fb}}(z) = \frac{\varepsilon_{*10,\text{UV}}(z) \varepsilon_{\text{esc},10} \eta_{\gamma*,\text{fid}} \left(\frac{\Omega_b}{\Omega_m} \right)}{t_H(z)} \times \int_{M_{\text{cool}}(z)}^{\infty} f_{\text{gas}}(M'_h) \left(\frac{M'_h}{10^{10}M_\odot} \right)^{\alpha_{\text{esc}} + \alpha_*} M'_h \frac{dn}{dM_h}(M'_h, z) dM'_h, \quad (2.7)$$

where

$$\varepsilon_{\text{esc},10} \equiv \frac{\mathcal{K}_{\text{UV}}}{\mathcal{K}_{\text{UV},\text{fid}}} \frac{\eta_{\gamma*}}{\eta_{\gamma*,\text{fid}}} f_{\text{esc},10}. \quad (2.8)$$

The corresponding yield from galaxies that are not affected by radiative feedback, $\dot{n}_{\text{ion}}^{\text{nofb}}(z)$, is obtained by setting $f_{\text{gas}}(M'_h) = 1$ in equation (2.7). In all cases, we assume that at any cosmic epoch, only halos with masses greater than the mass threshold $M_{\text{cool}}(z)$ for which atomic cooling becomes effective (i.e., $T_{\text{vir}} \geq 10^4$ K) contribute ionizing photons.

The total comoving number density of ionizing photons that leaks into the IGM per unit time at a given redshift z is therefore calculated as [55, 56] -

$$\dot{n}_{\text{ion}}(z) = Q_{\text{HII}}(z) \dot{n}_{\text{ion}}^{\text{fb}}(z) + [1 - Q_{\text{HII}}(z)] \dot{n}_{\text{ion}}^{\text{nofb}}(z) \quad (2.9)$$

We adopt a fiducial value of $\mathcal{K}_{\text{UV},\text{fid}} = 1.15485 \times 10^{-28} \text{M}_\odot \text{yr}^{-1}/\text{ergss}^{-1}\text{Hz}^{-1}$ and $\eta_{\gamma*,\text{fid}} = 4.62175 \times 10^{60}$ photons per M_\odot in all our calculations. These values were obtained using **STARTBURST99 v7.0.1**²[57] for a stellar population with a Salpeter IMF (0.1 - 100 M_\odot) and metallicity $Z = 0.001 (= 0.05 Z_\odot)$ at an age of 100 Myr, assuming continuous star formation. The assumed fiducial values for \mathcal{K}_{UV} and $\eta_{\gamma*}$ translate to an ionizing photon production efficiency $\log_{10} [\xi_{\text{ion},\text{fid}}/(\text{ergs}^{-1} \text{Hz})] \approx 25.23$.

In CC24, the parameters $\log_{10}(\varepsilon_{*10,\text{UV}})$ and α_* were considered to evolve with redshift following a tanh parameterization. In this work, we make the simplifying assumption that the transition redshift and the redshift width for this tanh evolution are identical for both parameters, that is, $z_\alpha = z_\varepsilon = z_*$ and $\Delta z_\varepsilon = \Delta z_\alpha = \Delta z_*$. Therefore, the respective redshift evolution are now given by

$$\log_{10}(\varepsilon_{*10,\text{UV}}) = \ell_{\varepsilon,0} + \frac{\ell_{\varepsilon,\text{jump}}}{2} \tanh\left(\frac{z - z_*}{\Delta z_*}\right), \quad (2.10)$$

and

$$\alpha_* = \alpha_0 + \frac{\alpha_{\text{jump}}}{2} \tanh\left(\frac{z - z_*}{\Delta z_*}\right). \quad (2.11)$$

In this formulation, the parameter $\log_{10} \varepsilon_{*10,\text{UV}}$ (α_*) asymptotes to $\ell_{\varepsilon,0} - \ell_{\varepsilon,\text{jump}}/2$ ($\alpha_0 - \alpha_{\text{jump}}/2$) at low redshifts and to $\ell_{\varepsilon,0} + \ell_{\varepsilon,\text{jump}}/2$ ($\alpha_0 + \alpha_{\text{jump}}/2$) at high redshifts, with the transition between these values occurring at a characteristic redshift z_* over a range Δz_* .

²<https://www.stsci.edu/science/starburst99/docs/default.htm>

Once the global reionization history $Q_{\text{HII}}(z)$ is obtained, the Thomson scattering optical depth of the CMB photons for that particular model is computed as

$$\tau_{el} \equiv \tau(z_{\text{LSS}}) = \sigma_T \bar{n}_H c \int_0^{z_{\text{LSS}}} \frac{dz'}{H(z')} (1+z')^2 \chi_{\text{He}}(z') Q_{\text{HII}}(z'), \quad (2.12)$$

where z_{LSS} is the redshift of last scattering, \bar{n}_H is the current mean comoving number density of hydrogen, and σ_T is the Thomson scattering cross-section. In practice, the integral in equation (2.12) does not pick up any contributions from redshifts before the onset of reionization z_{start} , as $Q_{\text{HII}}(z > z_{\text{start}}) = 0$.

Besides the observables discussed so far, one can also compute the effective number-weighted linear bias of galaxies $b_{\text{gal}}^{\text{eff}}$ at a redshift z from the model

$$b_{\text{gal}}^{\text{eff}}(z) = \frac{\int_{M_{\text{UV},\text{min}}}^{M_{\text{UV},\text{max}}} dM_{\text{UV}} \{Q_{\text{HII}}(z) b_{\text{gal}}^{\text{fb}}(M_{\text{UV}}, z) \Phi_{\text{UV}}^{\text{fb}} + [1 - Q_{\text{HII}}(z)] \Phi_{\text{UV}}^{\text{nofb}} b_{\text{gal}}^{\text{nofb}}(M_{\text{UV}}, z)\}}{\int_{M_{\text{UV},\text{min}}}^{M_{\text{UV},\text{max}}} dM_{\text{UV}} \{Q_{\text{HII}}(z) \Phi_{\text{UV}}^{\text{fb}} + [1 - Q_{\text{HII}}(z)] \Phi_{\text{UV}}^{\text{nofb}}\}}, \quad (2.13)$$

where $b_{\text{gal}}^{\text{fb}}(M_{\text{UV}}, z)$ and $b_{\text{gal}}^{\text{nofb}}(M_{\text{UV}}, z)$ represents the linear bias of galaxies, with absolute magnitude M_{UV} at redshift z , residing in ionized and neutral regions respectively and is calculated from the linear halo bias b_{halo} , as follows

$$\begin{aligned} b_{\text{gal}}^{\text{fb}}(M_{\text{UV}}, z) &= b_{\text{halo}} \left(M_h(M_{\text{UV}}) \Big|_{\text{fb}}, z \right) \\ b_{\text{gal}}^{\text{nofb}}(M_{\text{UV}}, z) &= b_{\text{halo}} \left(M_h(M_{\text{UV}}) \Big|_{\text{nofb}}, z \right). \end{aligned} \quad (2.14)$$

While calculating the effective bias, we take $M_{\text{UV},\text{max}}$ to be same as that adopted in the observational study under consideration and $M_{\text{UV},\text{min}} = -21$ ³. We use the fitting formula of Tinker et al. (2010) [35] to compute the linear halo bias b_{halo} .

To summarize, the **baseline** model of high-redshift star-forming galaxies has *nine* free parameters - $\theta = \{\ell_{\varepsilon,0} - \ell_{\varepsilon,\text{jump}}/2, \alpha_0 - \alpha_{\text{jump}}/2, \ell_{\varepsilon,0} + \ell_{\varepsilon,\text{jump}}/2, \alpha_0 + \alpha_{\text{jump}}/2, z_*, \Delta z_*, \alpha_{\text{esc}}, \log_{10}(\varepsilon_{\text{esc},10}), \log_{10}(M_{\text{crit}}/M_{\odot})\}$.

3 Observational Datasets and Likelihood Analysis

We utilize several available observational data sets to constrain the theoretical model described in the previous section through a Bayesian analysis. In this section, we briefly summarize them and also describe the Bayesian formalism used to constrain the free parameters of our model.

1. **Thomson scattering optical depth of CMB photons:** For our analysis, we use the latest measurement of $\tau_{el} = 0.054 \pm 0.007$ reported by the Planck collaboration [58].
2. **Global Reionization History:** We utilize measurements of the globally averaged neutral hydrogen fraction ($Q_{\text{HI}} = 1 - Q_{\text{HII}}$) in the IGM at different redshifts derived from Lyman- α absorption studies of distant quasars and galaxies, similar to our previous work [50]. It is essential to remember that all these constraints are however model-dependent.

³This is because our model does not account for the effects of active galactic nuclei (AGN) feedback or dust attenuation that are likely to affect the brighter galaxies.

3. **Galaxy UV Luminosity Functions:** We use measurements of the galaxy UV luminosity functions $\Phi_{\text{UV}}(M_{\text{UV}}, z)$ at nine redshift bins spanning the redshift range: $5 \leq z \leq 15$, obtained from various surveys conducted with the Hubble Space Telescope [59] and the James Webb Space Telescope [8–11]. In addition to the datasets used in CC24, we have included new JWST measurements at $z \geq 9$ [12] and the measurements from HST at $z = 5$ in this present work. As our theoretical model does not incorporate the effects of feedback from active galactic nuclei (AGN) activity or the significant dust attenuation present in bright galaxies, we consider only the observational data points with $M_{\text{UV}} \geq -21$ from these studies in our analysis [60].
4. **Galaxy Bias:** We use the most recent measurements of galaxy bias $b_{\text{gal}}(z)$ over the redshift range - $5.5 \leq z \leq 10.6$, derived from the angular clustering of UV-bright galaxies observed with the JWST [44]. While computing the galaxy bias from the theoretical model, we also impose the same magnitude cuts ($M_{\text{UV,max}}(z)$) as mentioned in their paper (refer to Figure 1 of [44] for the values at each z).

We use a Bayesian analysis to constrain the free parameters of our model by comparing the theoretical predictions with all or a subset of the observational constraints mentioned above. This involves computing the conditional probability distribution or the posterior $\mathcal{P}(\boldsymbol{\theta}|\mathcal{D})$ of the model parameters $\boldsymbol{\theta}$ given the observational data \mathcal{D} , using the Bayes theorem, as follows

$$\mathcal{P}(\boldsymbol{\theta}|\mathcal{D}) = \frac{\mathcal{L}(\mathcal{D}|\boldsymbol{\theta}) \pi(\boldsymbol{\theta})}{\mathcal{P}(\mathcal{D})}, \quad (3.1)$$

where $\mathcal{L}(\mathcal{D}|\boldsymbol{\theta})$ is the likelihood i.e. the conditional probability distribution of the data \mathcal{D} given the model parameters $\boldsymbol{\theta}$, $\pi(\boldsymbol{\theta})$ is the prior distribution of the parameters of the model, and $\mathcal{P}(\mathcal{D})$ is the model evidence which is redundant in our work. Assuming the datasets to be independent, the joint likelihood is calculated as

$$\mathcal{L}(\mathcal{D}|\boldsymbol{\theta}) = \prod_{\alpha} \mathcal{L}(\mathcal{D}_{\alpha}|\boldsymbol{\theta}), \quad (3.2)$$

where the index α runs over the datasets (among those mentioned above) that are used in a particular analysis and the likelihood for any individual dataset \mathcal{D}_{α} is given by

$$\mathcal{L}(\mathcal{D}_{\alpha}|\boldsymbol{\theta}) = \exp \left[-\frac{1}{2} \chi^2(\mathcal{D}_{\alpha}, \boldsymbol{\theta}) \right] = \exp \left[-\frac{1}{2} \sum_i \left(\frac{\mathcal{D}_{\alpha,i} - \mathcal{M}_{\alpha,i}(\boldsymbol{\theta})}{\sigma_{\alpha,i}} \right)^2 \right], \quad (3.3)$$

where $\mathcal{D}_{\alpha,i}$ are the values of the measured data points, $\sigma_{\alpha,i}$ are the associated observational error bars and $\mathcal{M}_{\alpha,i}(\boldsymbol{\theta})$ are the values predicted by the model corresponding to the parameter set $\boldsymbol{\theta}$. The index i runs over all data points in the dataset \mathcal{D}_{α} . In this work, we have $\mathcal{D}_{\alpha} \subseteq \{\Phi_{\text{UV}}(M_{\text{UV}}, z), \tau_{\text{el}}, Q_{\text{HI}}(z), b_{\text{gal}}(z)\}$.

We use the Monte Carlo Markov Chain (MCMC) method to compute the posterior distribution of the free parameters of the model. To sample the parameter space, we use the publicly available package COBAYA⁴ [61]. The samples are drawn using 8 parallel chains and the chains are assumed to have converged when the Gelman–Rubin $R - 1$ statistic becomes less than a threshold of 0.01. We discard the first 30% of the steps in the chains as ‘burn-in’ and use the rest for our analysis.

⁴<https://cobaya.readthedocs.io/en/latest/>

4 Results from the baseline model

In this section, we discuss the results obtained by comparing the theoretical predictions of the **baseline** model with the available observations. For this purpose we execute two variants of MCMC runs using different combinations of observational datasets, as mentioned below

- **UVLF+reion**: In this case, we use the first three of the observational data sets (i.e., UVLFs, $Q_{\text{HI}}(z)$ and τ_{el}) outlined in Section 3. This corresponds to the default case in CC24 and will enable us to constrain the updated **baseline** model using the new datasets.
- **bias+reion**: In this case, we substitute the observed UVLF datasets with the galaxy bias measurements, while retaining all the reionization observables for the likelihood analysis. The primary motivation behind this run is to understand the galaxy-halo connection required to match the galaxy bias measurements, while also ensuring consistency with the current constraints on the timeline of reionization.

We begin with the results obtained from the MCMC runs of the **UVLF+reion** case. The marginalized constraints on the free and derived parameters are mentioned in the third column of Table 1. We show the model-predicted UVLFs for 200 random samples from the MCMC chains in Figure 1, along with the observational measurements used in the MCMC analysis. The evolution in the efficiency parameters preferred by the data has been plotted in Figure 2 for the same 200 random samples. From Table 1, we find that an increase in the efficiency of production of UV radiation from galaxies is required at $z \geq 10$ to match the evolving UVLF observations from the JWST, while remaining approximately constant at lower redshifts down to $z = 5$. These findings are qualitatively similar to those reported in our earlier works (CC24). From the present analysis, we obtain improved constraints on the timing of this transition, which is expected to occur between $z \approx 10$ and $z \approx 12$ over a redshift interval of $\Delta z \approx 1 - 2$. Interestingly, the inclusion of the $z = 5$ UVLF observational data into the analysis helps in constraining the value of $\log_{10}(M_{\text{crit}}/M_{\odot}) \approx 10.07$. This is not surprising since the total UVLF at $z = 5$ predicted by our model is exactly equal to the UVLF from feedback-affected regions as hydrogen reionization is complete (i.e., $Q_{\text{HII}} = 1$) by then. The global reionization histories for the 200 random samples from the MCMC chains are shown in the left-hand panel of Figure 3. As a result of increased suppression in star formation due to stronger feedback, the model now requires a higher escape fraction for $10^{10} M_{\odot}$ halos (compared to that obtained in CC24) to remain consistent with the reionization observables. We also find that the inferred power-law index of the halo-mass dependent escape fraction is somewhat flatter compared to our earlier work, although still preferring negative values (at 68% confidence).

In the right-hand panel of Figure 3, we show a comparison of the redshift evolution of the effective galaxy bias predicted by the **UVLF+reion** model with the recent bias measurements obtained from JWST at $z \geq 5.5$ [44], keeping in mind that these measurements were not included while computing the posterior distribution using MCMC. Although our model captures the general trend of an increasing galaxy bias with redshift and is consistent with measurements at $z > 9$, it does not accurately reproduce the steep evolution inferred from observations and overestimates the galaxy bias at $z < 9$. Since galaxies residing in low-mass halos are expected to cluster less strongly than those in high-mass halos, this discrepancy between our model and clustering observations hints towards the fact that galaxies of fixed

Table 1: Parameter constraints obtained from the MCMC-based analysis. The first nine rows correspond to the free parameters of the **baseline** model while the remaining are the derived parameters. The free parameters are assumed to have uniform priors in the range mentioned in the second column. The numbers in the other columns show the mean value with 1σ errors for different parameters of the model, as obtained from the two MCMC runs (see Section 4).

Parameters	Priors	UVLF+reion	bias+reion
$\ell_{\varepsilon,0} + \ell_{\varepsilon,\text{jump}}/2$	[-2.0, 2.0]	$-0.238_{-0.36}^{-0.064}$	$-0.29_{-1.5}^{+0.68}$
$\ell_{\varepsilon,0} - \ell_{\varepsilon,\text{jump}}/2$	[-2.0, 1.0]	$-0.910_{-0.044}^{+0.069}$	$0.08_{-0.52}^{+0.46}$
z_*	[8.0, 18.0]	$11.62_{-1.3}^{+0.17}$	< 12.4
Δz_*	[0.5, 6.0]	$1.71_{-0.85}^{+0.29}$	> 3.7
$\alpha_0 + \alpha_{\text{jump}}/2$	[0.0, 7.0]	$1.8844_{-1.3}^{-0.0063}$	$3.9_{-1.3}^{+2.7}$
$\alpha_0 - \alpha_{\text{jump}}/2$	[-1.0, 1.0]	$0.303_{-0.050}^{+0.036}$	> -0.192
$\log_{10}(\varepsilon_{\text{esc},10})$	[-3.0, 1.0]	$-0.813_{-0.035}^{+0.042}$	$-1.93_{-0.43}^{+0.55}$
α_{esc}	[-3.0, 1.0]	$-0.18_{-0.11}^{+0.14}$	-0.78 ± 0.71
$\log_{10}(M_{\text{crit}}/M_{\odot})$	[9.0, 11.0]	$10.07_{-0.11}^{+0.30}$	< 10.1
τ_{el}	-	$0.0543_{-0.0024}^{+0.0020}$	$0.0523_{-0.0029}^{+0.0018}$
$\ell_{\varepsilon,\text{jump}}$	-	$0.673_{-0.40}^{-0.028}$	$-0.4_{-1.5}^{+1.0}$
α_{jump}	-	$1.58145_{-1.3}^{+0.00057}$	$3.8_{-1.7}^{+2.3}$

UV luminosity at $z = 5 - 8$ possibly populate occupy halos of lower mass than predicted by the model in this case.

To investigate the cause of this disagreement, we carried out an analysis, referred to as the **bias+reion** case, where the requirement for the galaxy-halo connection to match the galaxy UVLFs is relaxed. Instead, we focus on simultaneously fitting the **baseline** model to both the galaxy bias and the reionization observables (Q_{HI} and τ_{el}). The constraints on the model parameters for this case are mentioned in the fourth column of Table 1. Additionally, Figure 4 shows the evolution in galaxy bias and the reionization histories for 200 random

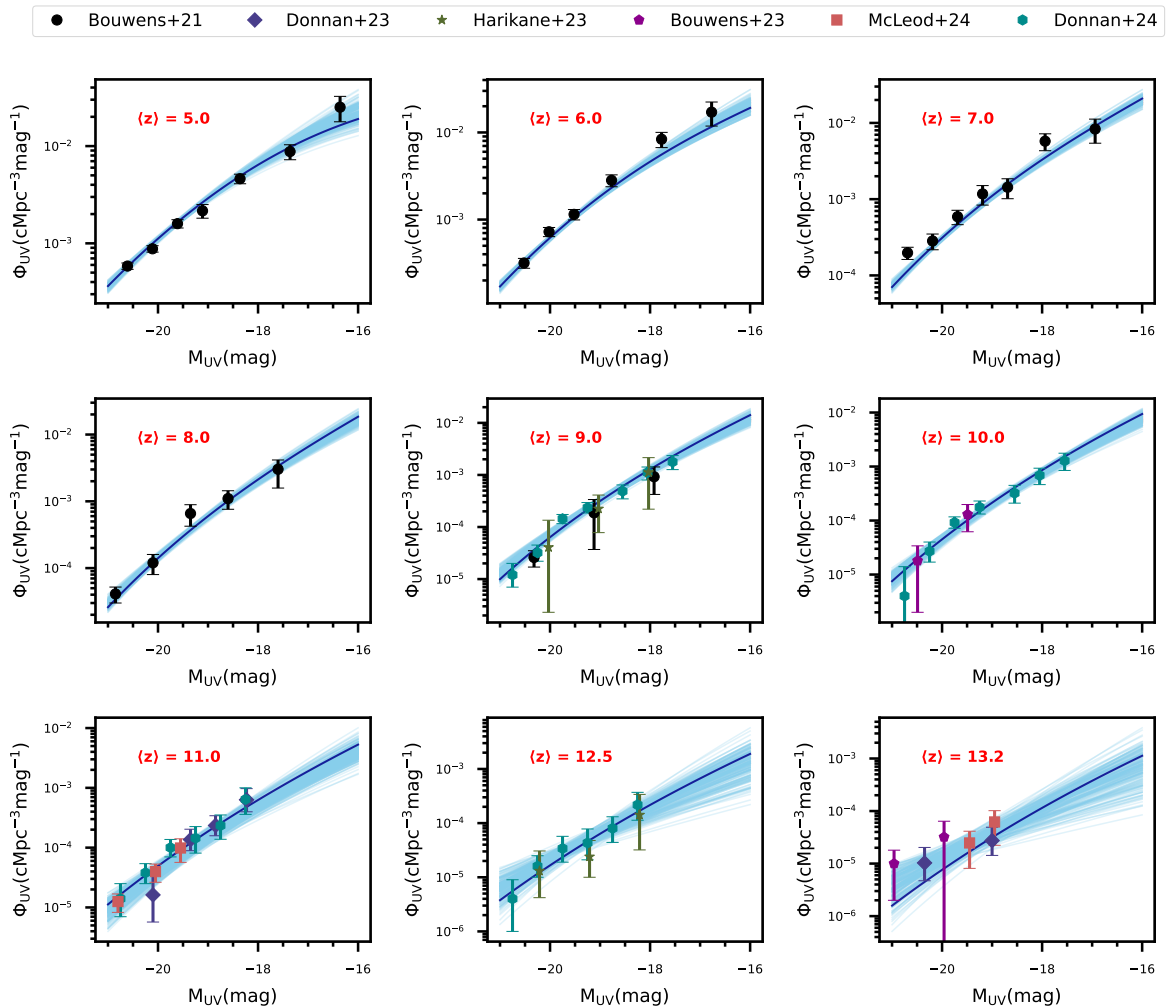


Figure 1: The galaxy UV luminosity functions at nine different redshift bins (with their respective mean values $\langle z \rangle$ mentioned in the upper left corner) for 200 random samples drawn from the MCMC chains of the **UVLF+reion** case. In each panel, the solid dark-blue line corresponds to the best-fit model, while the colored data points show the different observational constraints [8–12, 59] used in the likelihood analysis.

samples drawn from the MCMC chains of the **bias+reion** case alongside the corresponding observational measurements.

We find that the efficiency parameter $\varepsilon_{*10,UV}$ takes significantly higher values (compared to the **UVLF+reion** case) at lower redshifts and shows no preference for evolution with redshift, evident from the fact that $\ell_{\varepsilon,jump}$ is statistically consistent with zero. As a result of this increased UV efficiency, galaxies of a given UV luminosity are now accommodated within relatively lower mass, but more abundant, halos. The power-law index α_* also decreases at lower redshifts ($z \lesssim 10$), enhancing the efficiency of star formation (and thereby, UV emission) in low-mass halos. This too leads to UV-bright galaxies being hosted in lower mass halos. Consequently, while this galaxy-halo connection helps the model to match the galaxy bias observations at $z \leq 9$, it leads to an overestimation of the abundances of UV galaxies at all magnitude bins over the same range of redshifts, as illustrated in Figure 5. Furthermore, in

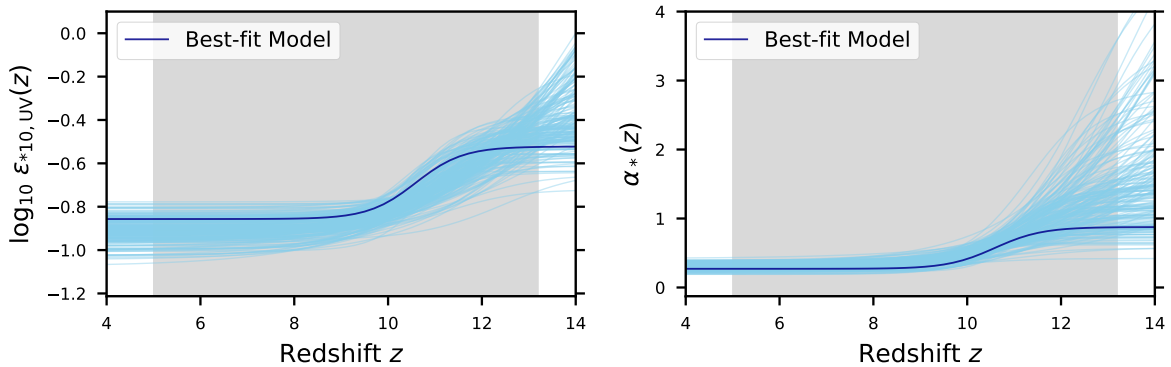


Figure 2: The redshift evolution of the normalization (left panel) and power-law (right panel) scaling of the production efficiency of UV radiation with halo mass for 200 random samples drawn from the MCMC chains of the **UVLF+reion** case. The grey box encloses the range of average redshifts ($5 \leq \langle z \rangle \leq 13.2$) at which UVLF observations have been used for comparison with the model in this work.

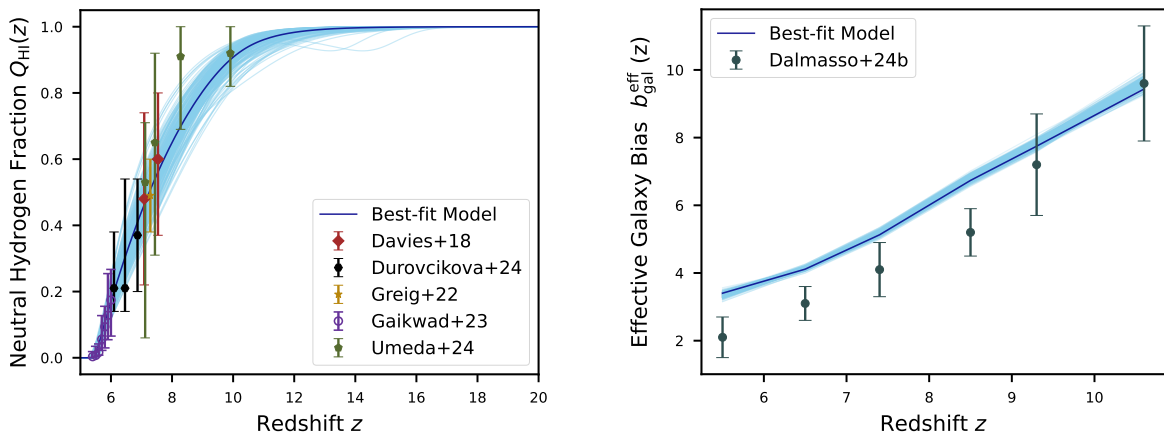


Figure 3: The evolution of the globally averaged intergalactic neutral hydrogen fraction (left panel) and the effective galaxy bias (right panel) as a function of redshift for 200 random samples drawn from the MCMC chains of the **UVLF+reion** case. The colored data points in the left and right panels represent the observed measurements for $Q_{\text{HI}}(z)$ and $b_{\text{gal}}^{\text{eff}}(z)$, respectively. Note that, unlike the reionization history, the galaxy bias observations are not included in the likelihood analysis for the **UVLF+reion** case.

order to satisfy the reionization observables, the model requires these over-luminous galaxies to have extremely low escape fractions — around 1% – 2% in the case of $10^{10} M_{\odot}$ halos.

From the discussions in this section, it is evident that the **baseline** model struggles to simultaneously reproduce the observed galaxy UVLF and bias. Therefore, our next step is to explore extensions or modifications to the **baseline** model, aiming to reconcile both summary statistics (the galaxy UVLF and bias) within a consistent physical framework. We discuss this in the next section.

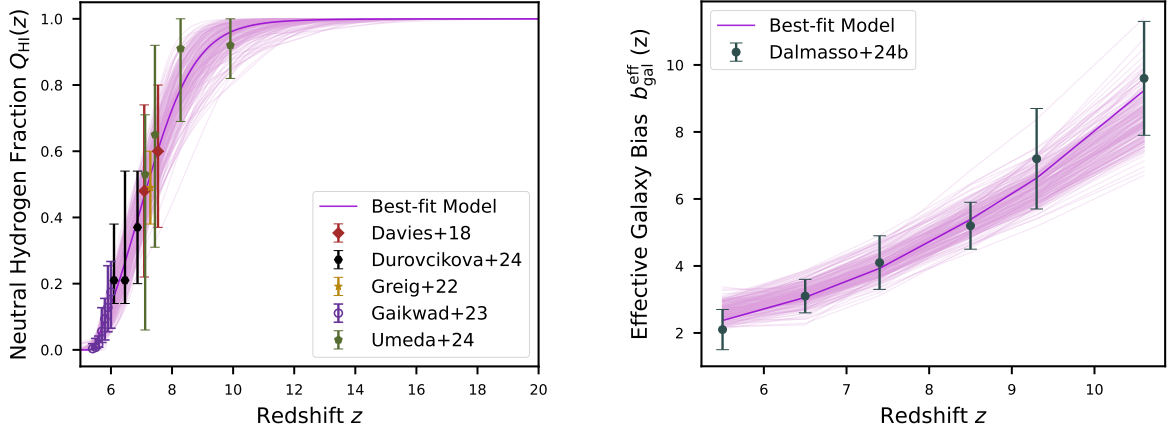


Figure 4: Same as Figure 3 but for 200 random samples drawn from the MCMC chains of the **bias+reion** case. Note that the likelihood analysis for the **bias+reion** case includes both the reionization history and galaxy bias observations, whereas the UVLf datasets were excluded.

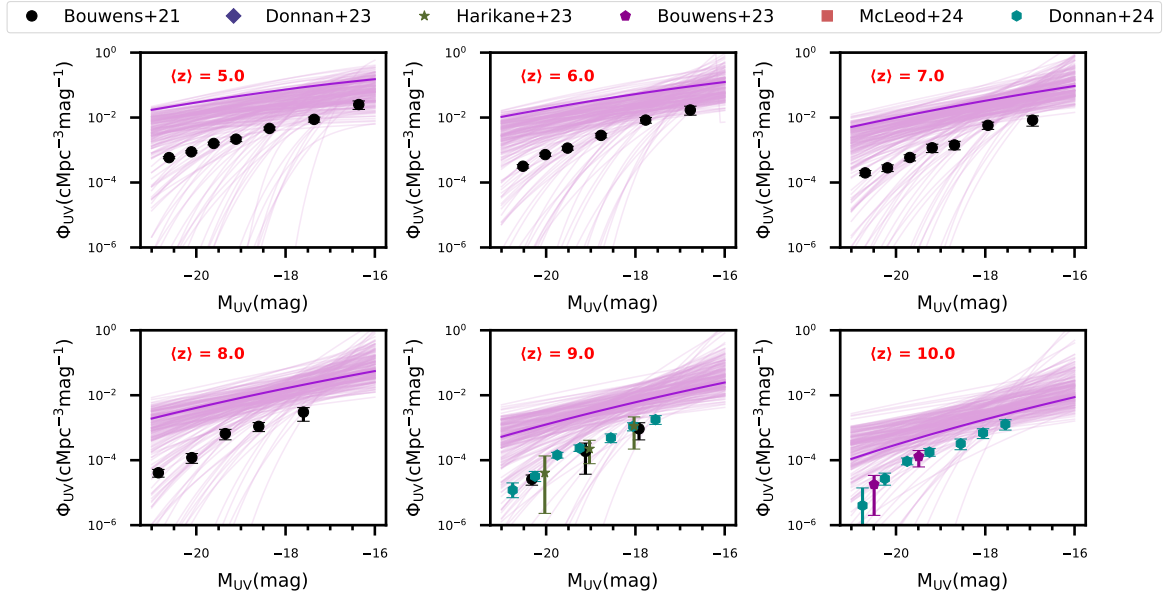


Figure 5: The *predicted* galaxy UV luminosity functions at $5 \leq z \leq 10$ for 200 random samples drawn from the MCMC chains of the **bias+reion** case. In each panel, the solid dark-violet line corresponds to the best-fit model, while the colored data points show the different observational constraints [8–12, 59]

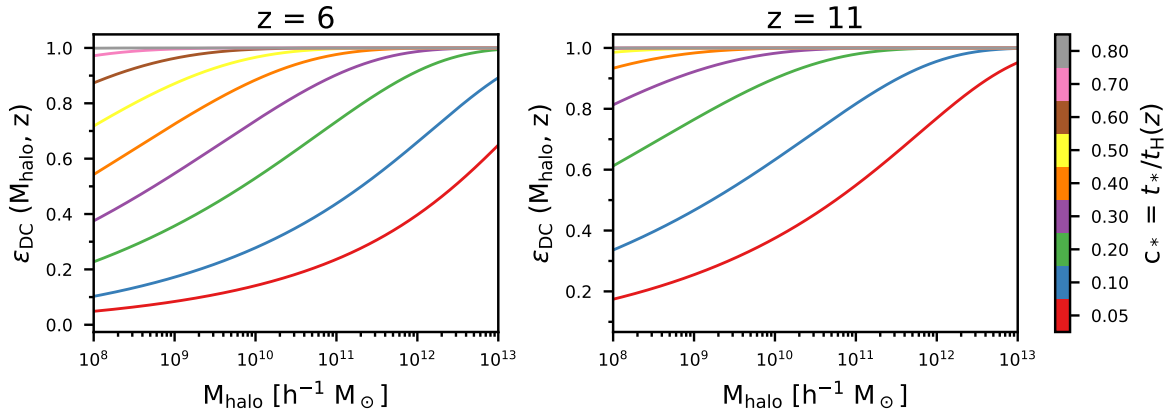


Figure 6: The effective duty cycle as a function of halo mass at two representative redshifts for different values of c_* .

5 Extensions to the baseline model: Inclusion of duty cycle

A potential solution to address the surplus of UV-emitting galaxies that arises while tuning our **baseline** model to match the clustering measurements is to introduce a duty cycle, which would result in only a fraction of the underlying galaxy population being “observable” at any given time. We assume that, at any redshift, only those halos that formed within a given preceding time interval Δt will be able to host ‘detectable’ UV-bright galaxies, thereby naturally yielding a duty cycle that depends on both redshift and halo mass. This is motivated by the fact that a recent increase in mass, particularly due to mergers, within a halo can correlate with episodes of intense star formation that boosts the UV emission from the resident galaxy. In this work, we adopt the duty cycle parameterization of Trenti et al. (2010) [14], wherein the fraction (ϵ_{DC}) of dark-matter halos of a particular mass that host detectable UV-bright galaxies at a given cosmic time is given by

$$\epsilon_{DC}(\Delta t, M_h, z) = \frac{\int_{M_h}^{+\infty} \left[\frac{dn}{dM_h}(M'_h, z) - \frac{dn}{dM_h}(M'_h, z_{\Delta t}) \right] dM'_h}{\int_{M_h}^{+\infty} \frac{dn}{dM_h}(M'_h, z) dM'_h}. \quad (5.1)$$

where $\Delta t = t_H(z) - t_H(z_{\Delta t})$.

Incorporating an effective duty cycle into the model impacts the calculation of the UV luminosity function (equation (2.6)) and the ionizing emissivity (equation (2.7)) by modifying the occupancy of dark matter halos through the following transformation

$$\frac{dn}{dM_h}(M'_h, z) \rightarrow \epsilon_{DC}(M'_h, z) \frac{dn}{dM_h}(M'_h, z) \quad (5.2)$$

From equation (5.1), it is evident that the limiting case of $\epsilon_{DC}(M_h, z) = 1$ is recovered when $\Delta t \rightarrow \infty$. We assume that this timescale, Δt , which is associated with the global evolution of the HMF, to be equal to the star formation timescale $t_*(z) = c_*(z) t_H(z)$. The resulting theoretical model, involving a non-unity duty cycle, will henceforth be referred to as the **extended** model.

In our **extended** model, the star-formation time scale t_* (or equivalently, c_*) plays two important roles. It not only determines the duty cycle of halos, but also affects the UV luminosity of the galaxy occupying it, as given by equations (2.2) and (2.3). For example, decreasing the value of c_* at any redshift results in low-mass halos housing increasingly brighter galaxies. However, this is accompanied by a corresponding decrease in the number of these galaxies that will be eventually detectable (at any given time).

Furthermore, this prescription of duty cycle helps break the degeneracy between some of the parameters governing the production efficiency of UV radiation, namely between t_* and $f_{*,10}(\mathcal{K}_{\text{UV, fid}}/\mathcal{K}_{\text{UV}})$. These parameters had previously appeared in a degenerate multiplicative combination in the **baseline** model as the UV efficiency parameter $\varepsilon_{*,10,\text{UV}}$ (see equation (2.4)).

We show the variation of the effective duty cycle with halo mass and redshift for different values of c_* in Figure 6. For a fixed value of c_* , we find that the effective duty cycle increases with both halo mass, reflecting the rapid evolution of the high-mass end of the halo mass function, and with redshift, as halos of any given mass assemble more quickly at earlier times. Additionally, the duty cycle for halos at a fixed redshift also increases with an increase in the value of c_* , due to the larger number of halos forming within the extended time interval. In principle, the proportionally constant c_* , a new free parameter of our extended model, can even be a function of redshift. To accommodate enough flexibility in the model, we adopt a power-law redshift evolution for c_* as follows

$$c_*(z) = \min \left[0.5, c_{*,6} \left(\frac{1+z}{7} \right)^{\beta_{c_*}} \right] \quad (5.3)$$

where we limit $c_*(z)$ to a value less than 0.5.

As we will see later, the redshift evolution of $c_*(z)$ favored by the data makes this cut-off essential in preventing excessively prolonged episodes of star formation at high redshifts, ensuring that $t_*(z) \ll t_{\text{H}}(z)$. This particular choice of the cut-off value is motivated by the fact that for higher values of c_* , the duty cycle approaches unity across all relevant halo masses at $z \approx 11$. Beyond this redshift, where galaxy clustering data is unavailable, values of c_* higher than 0.5 and $f_{*,10}(\mathcal{K}_{\text{UV, fid}}/\mathcal{K}_{\text{UV}})$ are completely degenerate in their effect on the UV luminosity function (UVLF), since the duty cycle has already saturated. As a result, they cannot be independently constrained by the UVLF observations at $z > 11$.

For the redshift evolution of the parameter $f_{*,10}(\mathcal{K}_{\text{UV, fid}}/\mathcal{K}_{\text{UV}})$, we retain the tanh parameterization introduced earlier for $\varepsilon_{*,10,\text{UV}}$ but use different notations to avoid any confusion.

$$\log_{10} \left[f_{*,10} \left(\frac{\mathcal{K}_{\text{UV, fid}}}{\mathcal{K}_{\text{UV}}} \right) \right] = f_{\kappa,0} + \frac{f_{\kappa,\text{jump}}}{2} \tanh \left(\frac{z - z_*}{\Delta z_*} \right) \quad (5.4)$$

In terms of free parameters, the extended model involves *eleven* free parameters — two more in number ($c_{*,6}$ and β_{c_*}) compared to the baseline model.

We now proceed to discuss the results obtained from comparing the theoretical predictions of the **extended** model with the **all** observational datasets mentioned in Section 3. We refer to this case as the **UVLF+bias+reion** case.

While performing parameter inference for the **extended** model, we note that the disproportionately large number of data points in the UVLF dataset compared to the galaxy bias dataset causes a standard MCMC analysis using the joint likelihood defined in equation (3.2) to prioritize reproducing the UVLF measurements and place less emphasis on matching the

bias measurements. To circumvent this issue, we assign additional weight (w) to the galaxy bias dataset in the likelihood calculation. In this case, the joint likelihood takes the following form

$$\begin{aligned} \mathcal{L}(\mathcal{D}|\boldsymbol{\theta}) &= \prod_{\alpha} \exp \left[-\frac{1}{2} \chi^2(\mathcal{D}_{\alpha}, \boldsymbol{\theta}) \right] \\ &= -\frac{1}{2} \left[\chi^2(\mathcal{D}_{\Phi_{\text{UV}}}, \boldsymbol{\theta}) + w^2 \chi^2(\mathcal{D}_{b_{\text{gal}}}, \boldsymbol{\theta}) + \chi^2(\mathcal{D}_{Q_{\text{HI}}}, \boldsymbol{\theta}) + \chi^2(\mathcal{D}_{\tau_{\text{el}}}, \boldsymbol{\theta}) \right] \end{aligned} \quad (5.5)$$

We present results for the case where the weight factor is set to $w = 5$, a choice that seems adequate to reasonably match observations of both the galaxy summary statistics considering the relative proportion of their respective data points. The posterior distributions of the free parameters are shown in Figure 7, along with their mean values and 68% confidence intervals mentioned above the respective one-dimensional posterior distributions. We show a comparison between the UVLFs, reionization histories, and galaxy bias for 200 random samples drawn from the MCMC chains of **UVLF+bias+reion** case in Figures 8 and 9, along with the presently available observational measurements. The evolution of the different redshift-dependent free parameters of the model is shown in the top row of Figure 10.

From Figure 7 as well as the bottom-right panel of Figure 10, we find that to match all the observables, star-formation timescale in halos hosting UV-bright galaxies must evolve with redshift, rising from a value of ≈ 80 Myr at $z \approx 6$ steeply to around 120 Myr at $z \approx 8$. This implies a corresponding evolution in the population-averaged duty cycle with redshift since the star-formation timescale of a halo also determines its duty cycle in our model. Such a rising trend is qualitatively consistent with the findings of Dalmasso et al. (2024) [44] (see Table 1 of their paper) based on abundance matching techniques. The physical reason behind this increasing trend in the star-formation timescale remains unclear but may be linked to enhanced metal cooling, which facilitates more efficient star formation at relatively lower redshifts. Beyond $z = 12$, the fraction of dark matter halos hosting detectable UV-bright galaxies (for the mass range relevant for this study) is practically close to 100 % for the preferred values of c_* ($\gtrsim 0.4$).

In scenarios where star formation is spread out over shorter timescales, halos can host exceptionally UV-luminous galaxies, even with moderate star-formation efficiency. Consequently, at a fixed UV luminosity, galaxies will occupy comparatively less massive halos and therefore have lower bias. However, only a fraction of these abundant low-mass halos would have recently experienced star formation and thus host UV-bright galaxies. The **extended** model leverages this interplay to reconcile its predictions with both the galaxy UVLF and bias measurements at $z \leq 10$.

Interestingly, in the case of the **extended** model - where the mass-dependent duty cycle and UV luminosity are parameterized in terms of t_* , we notice that parameters such as f_{esc} and f_* no longer prefer additional dependence on halo mass to match the observed data. For instance, the power-law index of the star-formation efficiency at lower redshifts ($\alpha_0 - \alpha_{\text{jump}}/2$) is consistent with zero. However, to explain the surplus abundance and clustering of UV-bright galaxies at $z \geq 10$, an increase in the efficiency of star formation ($f_{*,10}$ and α_*) or production of UV light per unit star formation ($\mathcal{K}_{\text{UV, fid}}/\mathcal{K}_{\text{UV}}$) becomes necessary.

Moreover, with the mass-dependent duty cycle significantly reducing the occupancy of low-mass halos (see Figure 6), the critical mass M_{crit} associated with radiative feedback remains unconstrained (within the assumed prior interval), favouring values smaller than $10^9 M_{\odot}$. We further find that a constant escape fraction, independent of halo mass, of $\approx 12\%$

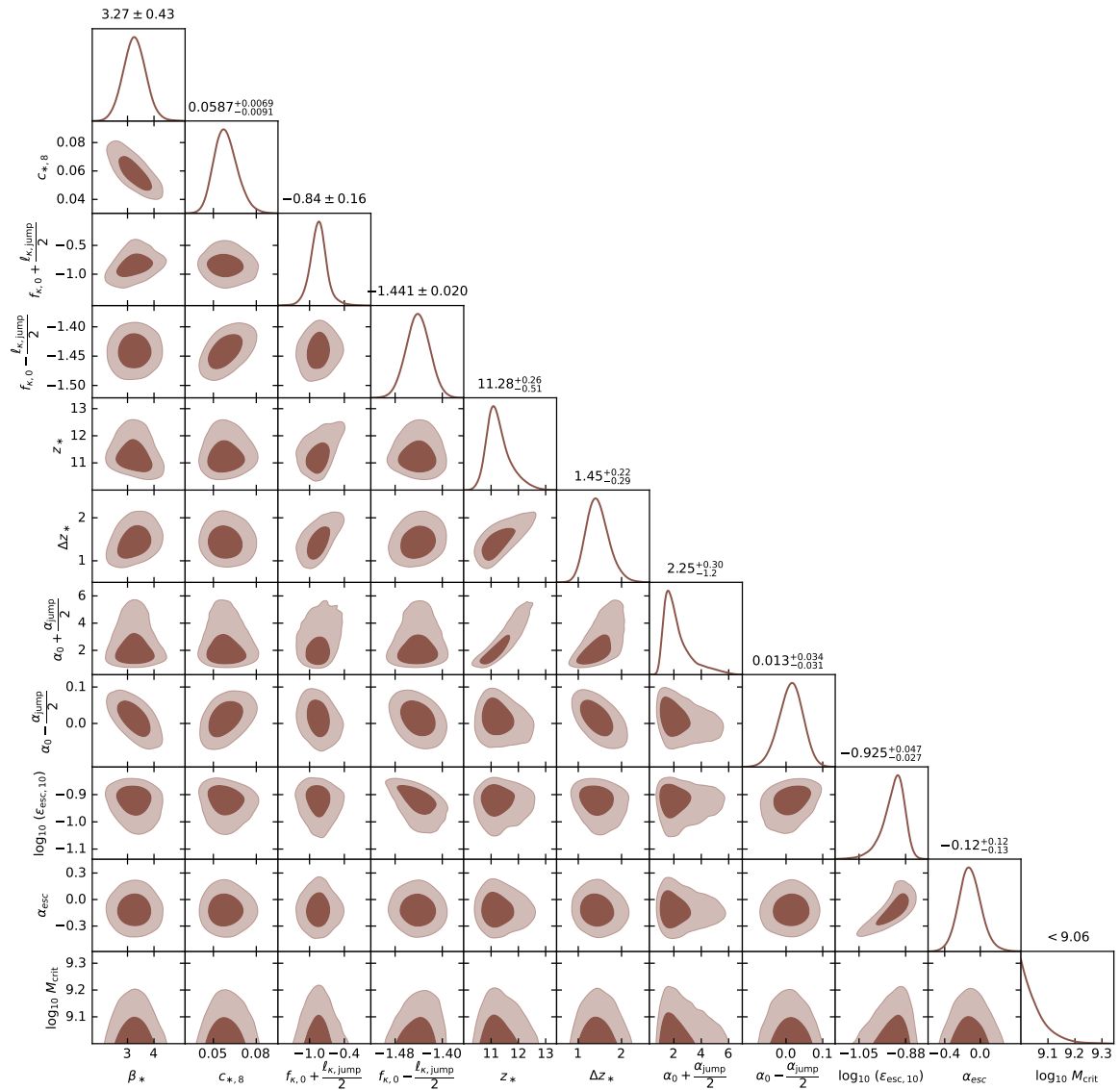


Figure 7: Posterior distributions of the free parameters for the **UVLF+reion** case. The diagonal panels show the one-dimensional posterior distribution, while the contour plots in the off-diagonal panels represent the two-dimensional joint distribution. The contour levels represent 68% and 95% confidence levels. The mean and 68% confidence intervals are denoted above the one-dimensional posterior distributions of the respective parameters.

(corresponding to the fiducial value of ξ_{ion} assumed in our model) produces reionization histories that are in agreement with current constraints.

While our analysis constrains the evolution of the star formation timescale by comparing the predictions of the **extended** model with observed galaxy UVLFs and clustering, these observations do not individually constrain the parameters - $f_{*,10}$ and $\mathcal{K}_{\text{UV,fid}}/\mathcal{K}_{\text{UV}}$ but only their product. In this regard, other galaxy summary statistics, such as the galaxy stellar mass function (GSMF) that offer a more direct measure of the star-formation efficiency compared to the UVLFs, can help in further breaking the degeneracy between $f_{*,10}$ and $\mathcal{K}_{\text{UV,fid}}/\mathcal{K}_{\text{UV}}$.

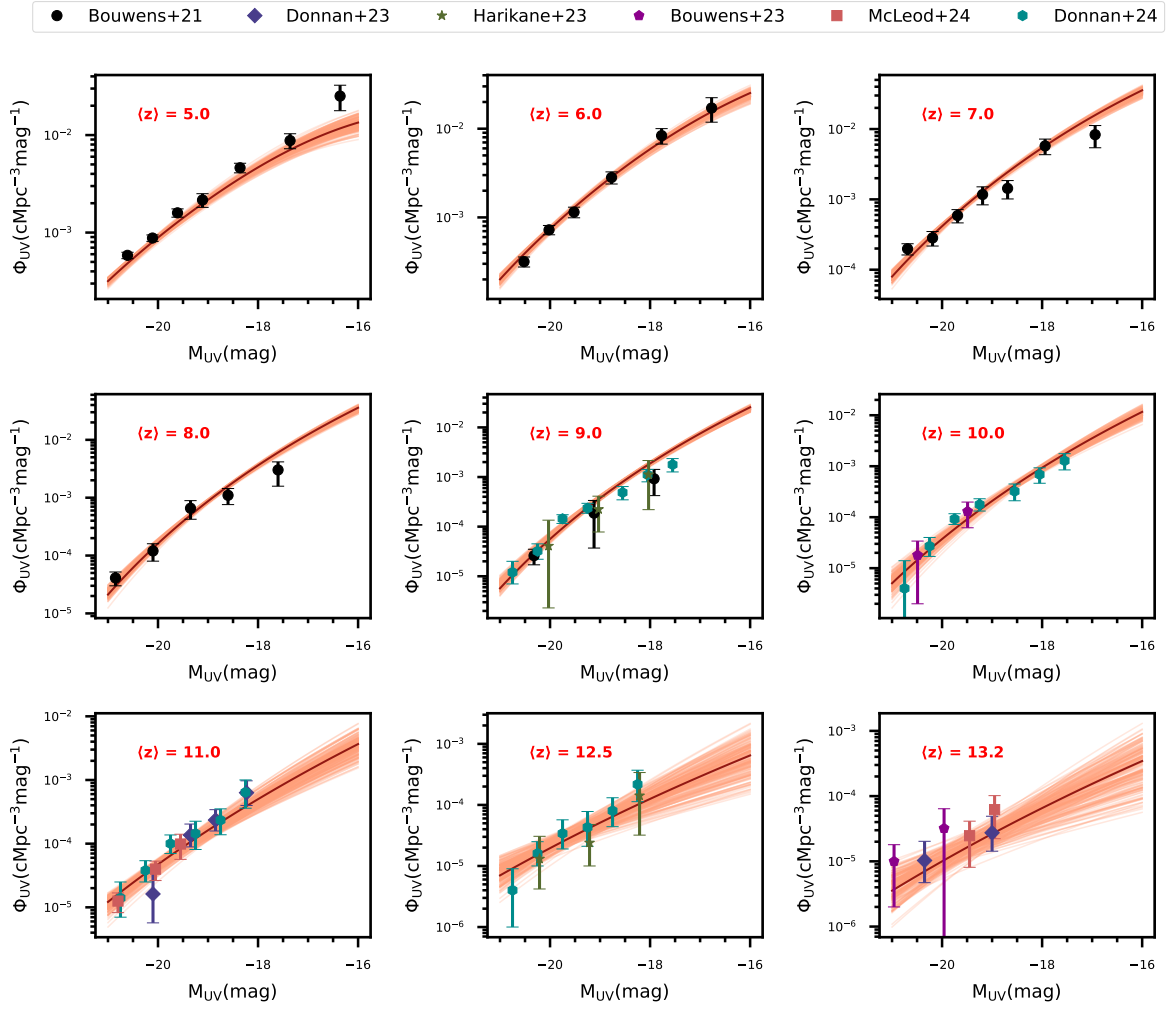


Figure 8: Same as Figure 1 but for 200 random samples drawn from the MCMC chains of the **UVLF+*bias*+*reion*** case with the **extended** model.

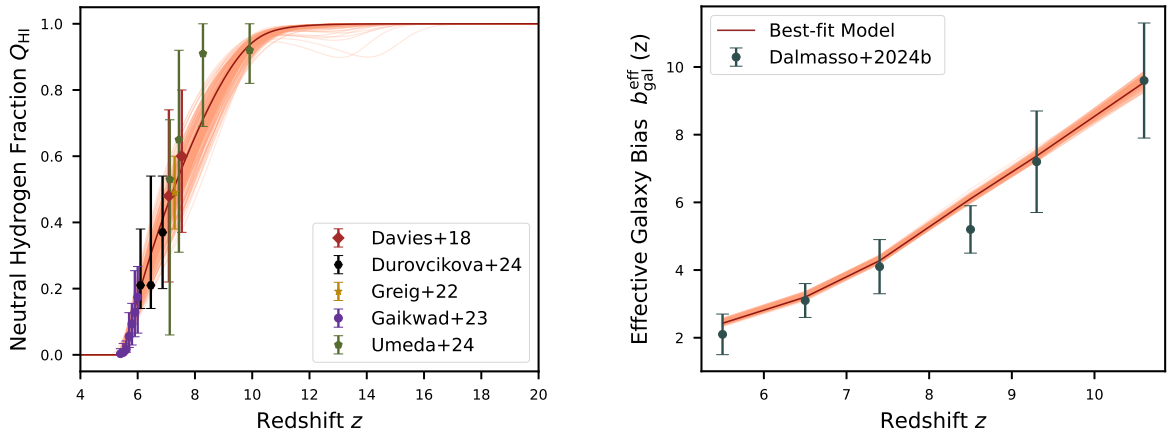


Figure 9: Same as Figure 3 but for 200 random samples drawn from the MCMC chains of the **UVLF+*bias*+*reion*** case with the **extended** model.

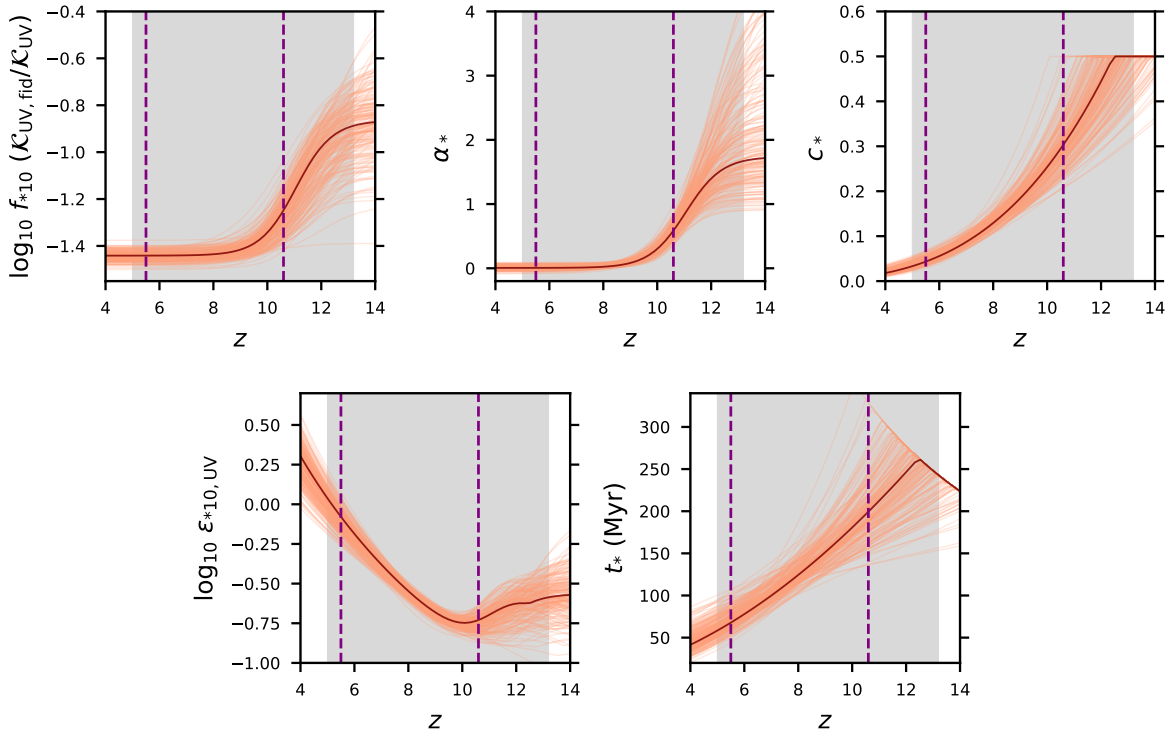


Figure 10: The redshift evolution of the normalization (top-left panel) and power-law (top-middle panel) scaling of the star-formation efficiency with halo mass and the star-formation timescale, in units of the local Hubble time, (top-right panel) for 200 random samples drawn from the MCMC chains of the **UVLF+bias+reion** case with the **extended** model. In each panel, the grey box and the vertical purple dashed lines encloses the redshift ranges used for comparing the model with UVLF ($5 \leq \langle z \rangle \leq 13.2$) and galaxy bias ($5.5 \leq \langle z \rangle \leq 10.6$) observations, respectively. In the bottom row, we also show the evolution of the “derived” parameters - $\varepsilon_{*10, \text{UV}}$ and $t_* = c_*(z) t_H(z)$, with redshift from the **extended** model for comparison to the earlier models.

However, it is important to realize that constructing the GSMF from observations is fraught with several uncertainties and systematic issues associated with estimating stellar masses from UV light. While we refrained from including the observational estimates of the GSMF in our likelihood calculations for these reasons, we now explore the insights that can be obtained by comparing the observed GSMF with that derived from our theoretical model, which already successfully matches other galaxy observations such as the UVLFs and large-scale bias.

In our model, the UV luminosity of a galaxy and its stellar mass are related as follows

$$L_{\text{UV}}(M_h, z) = \frac{1}{\mathcal{K}_{\text{UV}}} \frac{M_*(M_h, z)}{t_*(z)} \quad (5.6)$$

Therefore, the only input needed for converting the galaxy UV luminosity function to galaxy stellar mass function is \mathcal{K}_{UV} (more specifically, the ratio $\mathcal{K}_{\text{UV, fid}}/\mathcal{K}_{\text{UV}}$) since we have already obtained constraints on $c_*(z)$ and $f_{*,10}(\mathcal{K}_{\text{UV, fid}}/\mathcal{K}_{\text{UV}})$ by comparing the model predictions to the galaxy UVLF and bias observations. As mentioned earlier, this parameter \mathcal{K}_{UV} , which

depends on the properties of the stellar population and the recent star-formation history, is related to the mass-to-light ratio of galaxies in our model.

$$\mathcal{K}_{\text{UV, fid}}/\mathcal{K}_{\text{UV}} \approx 0.65$$

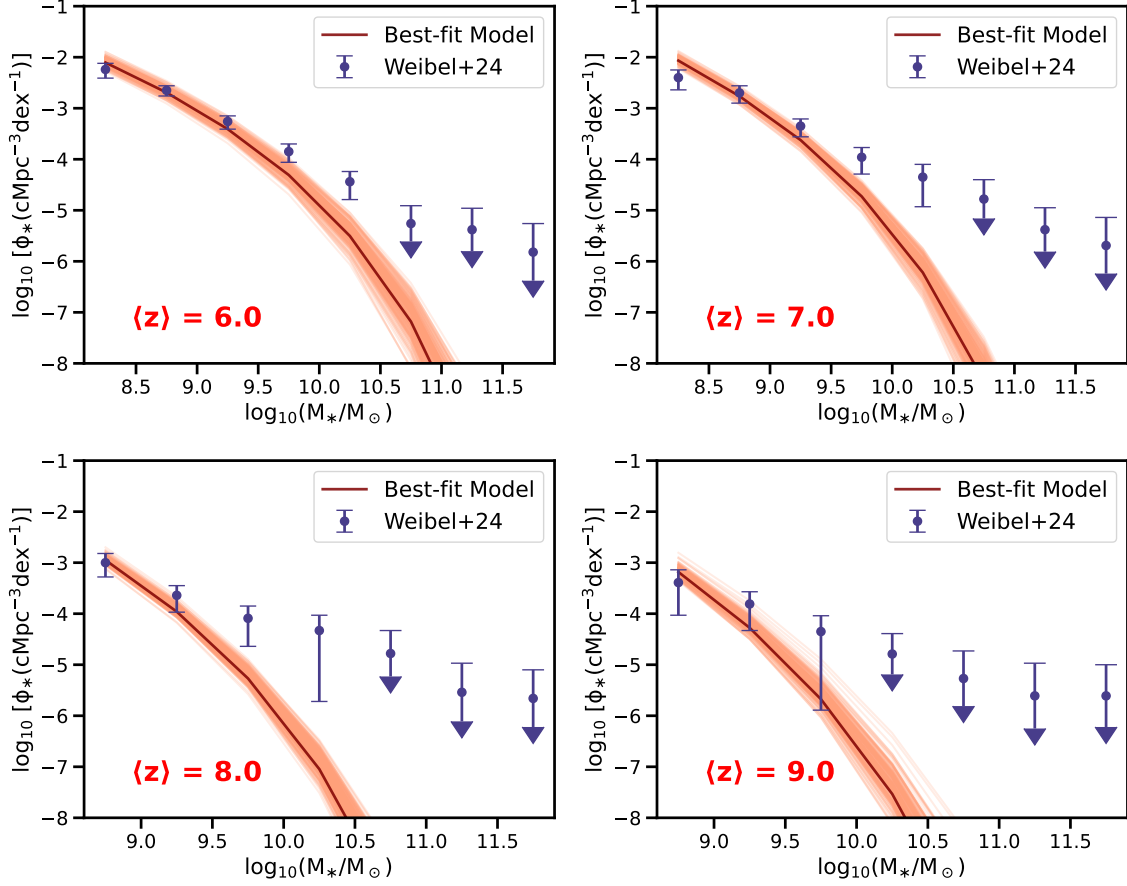


Figure 11: The derived galaxy stellar mass function (with $\mathcal{K}_{\text{UV, fid}}/\mathcal{K}_{\text{UV}} \approx 0.65$) corresponding to the best-fit model and 200 random samples from the MCMC chains of the **UVLF+bias+reion** case with the **extended** model shown in Figure 8.

For the models shown in Figure 8, we simply vary the ratio $\mathcal{K}_{\text{UV, fid}}/\mathcal{K}_{\text{UV}}$ until the derived galaxy stellar mass function shows agreement with the observational estimates of the SMF obtained from JWST [62]. We find that setting $\mathcal{K}_{\text{UV, fid}}/\mathcal{K}_{\text{UV}} \approx 0.65$ gives a reasonably good visual match to the data, as shown in Figure 11. However, the derived SMFs appear to underpredict the number of galaxies at very high stellar masses compared to observations, though the data points at these masses are only upper limits. The most significant mismatch between our predictions and observations occurs at $M_* \sim 10^{9.5} - 10^{10} M_\odot$, suggesting either an evolution of the mass-to-light ratio with stellar mass or the limitations of our UVLF model in dealing with brighter galaxies. In this regard, it is worth mentioning that the ratio of $\mathcal{K}_{\text{UV, fid}}/\mathcal{K}_{\text{UV}}$ obtained from our analysis is roughly about ~ 0.5 times the value commonly used in rescaling stellar mass estimates due to different IMFs (Salpeter in our model vs. Kroupa in the observational study) but perhaps remains plausible given additional

differences in the choice of the star formation history (continuous vs. delayed- τ SFH) and stellar population synthesis models (STARBURST99 vs. BPASS-v2.2.1) between our study and that assumed in Weibel et al. (2024) [62] while deriving the stellar masses from UV observations. From this simple proof-of-principle exercise with the **extended** model, we infer that a star formation efficiency ($f_{*,10}$) of approximately 5% produces a reasonable match to all the three galaxy observables (the galaxy stellar mass function, the galaxy UV luminosity function, and the large-scale galaxy bias) at $z < 10$.

6 Conclusion

The unprecedented wealth of observational data from space-based telescopes such as HST and JWST has revolutionized our understanding of galaxy formation and evolution during the first billion years of cosmic history. These observations are also crucial in characterizing the role of early star-forming galaxies in reionizing the Universe, providing stringent tests for theoretical models of high-redshift galaxy populations.

In this study, we leverage the theoretical framework of Chakraborty & Choudhury (2024) (CC24), which self-consistently links galaxy evolution and reionization, to extract key insights into the astrophysical properties of early galaxies during the Epoch of Reionization. Our main findings can be summarized as follows:

- Using an updated version of the CC24 model with nine free parameters, governing star formation efficiency, radiative feedback suppression, and ionizing photon escape fractions, we compare theoretical predictions against the latest JWST and HST measurements of the UV luminosity function (UVLF) at $z \sim 5 - 15$, as well as constraints from reionization, including the optical depth (τ_{el}) and the globally averaged neutral hydrogen fraction. Our results suggest that reconciling JWST’s UVLF measurements at $z \geq 10$ requires either more efficient star formation or higher UV radiation production per unit stellar mass. Additionally, our analysis supports scenarios in which faint, low-mass galaxies with higher escape fractions dominate cosmic reionization, aligning well with current constraints on the ionization history of the intergalactic medium (IGM).
- However, while our baseline model successfully connects UV luminosity to halo mass using UVLFs, it fails to reproduce the evolution of large-scale galaxy bias observed by JWST over $5 < z < 11$. Bias measurements at $5 < z < 9$ suggest that galaxies at fixed luminosity reside in lower-mass halos than predicted, leading to an overestimation of galaxy abundance in standard models.
- To address this discrepancy, we introduce a mass-dependent duty cycle, assuming that only galaxies in recently assembled halos, formed within the characteristic star-formation timescale at each epoch, remain bright in the UV. This naturally leads to a declining duty cycle at $z < 9$, while causing galaxies to appear brighter at fixed halo mass and reconciling the model with both UVLF and bias observations. Furthermore, assuming a mass-independent escape fraction of $\sim 12\%$, this extended model remains consistent with current reionization constraints.

These results highlight the necessity of incorporating higher-order summary statistics, such as large-scale galaxy bias, alongside conventional one-point statistics like the UV luminosity function to refine theoretical models of the galaxy-halo connection at high redshifts.

Our study demonstrates that a simple luminosity-based mapping to halo mass is insufficient and that the interplay between star formation timescales, halo assembly, and feedback must be carefully modeled to fully capture the evolution of early galaxies.

Future improvements to our model could further enhance its predictive power. The current approach, which assumes a constant mass-to-light ratio to estimate stellar masses, may not fully reproduce the observed stellar mass function, necessitating a more detailed treatment of galaxy star formation histories. Additionally, incorporating spatial fluctuations in the ionized hydrogen field would allow direct comparisons with Lyman- α opacity variations at $z \sim 5 - 6$ and upcoming 21 cm fluctuation experiments, requiring a transition to a semi-numerical framework. Lastly, improved constraints on galaxy clustering at high redshifts would provide further insights into the nature of early galaxy formation, enabling tighter constraints on the astrophysical parameters governing reionization.

Acknowledgments

The authors acknowledge support from the Department of Atomic Energy, Government of India, under project no. 12-R&D-TFR-5.02-0700.

Data Availability

The data generated and presented in this paper will be made available upon reasonable request to the corresponding author.

References

- [1] R.H. Wechsler and J.L. Tinker, *The Connection Between Galaxies and Their Dark Matter Halos*, *ARA&A* **56** (2018) 435 [[1804.03097](#)].
- [2] R.J. Bouwens, G.D. Illingworth, P.A. Oesch, M. Trenti, I. Labbé, L. Bradley et al., *UV Luminosity Functions at Redshifts $z \sim 4$ to $z \sim 10$: 10,000 Galaxies from HST Legacy Fields*, *ApJ* **803** (2015) 34 [[1403.4295](#)].
- [3] R.J. Bouwens, P.A. Oesch, G.D. Illingworth, R.S. Ellis and M. Stefanon, *The $z \sim 6$ Luminosity Function Fainter than -15 mag from the Hubble Frontier Fields: The Impact of Magnification Uncertainties*, *ApJ* **843** (2017) 129 [[1610.00283](#)].
- [4] H. Atek, J. Richard, J.-P. Kneib and D. Schaerer, *The extreme faint end of the UV luminosity function at $z \sim 6$ through gravitational telescopes: a comprehensive assessment of strong lensing uncertainties*, *MNRAS* **479** (2018) 5184 [[1803.09747](#)].
- [5] Y. Ono, M. Ouchi, Y. Harikane, J. Toshikawa, M. Rauch, S. Yuma et al., *Great Optically Luminous Dropout Research Using Subaru HSC (GOLDRUSH). I. UV luminosity functions at $z \sim 4$ -7 derived with the half-million dropouts on the 100 deg² sky*, *PASJ* **70** (2018) S10 [[1704.06004](#)].
- [6] R.A.A. Bowler, M.J. Jarvis, J.S. Dunlop, R.J. McLure, D.J. McLeod, N.J. Adams et al., *A lack of evolution in the very bright end of the galaxy luminosity function from $z = 8$ to 10*, *MNRAS* **493** (2020) 2059 [[1911.12832](#)].
- [7] Y. Harikane, Y. Ono, M. Ouchi, C. Liu, M. Sawicki, T. Shibuya et al., *GOLDRUSH. IV. Luminosity Functions and Clustering Revealed with 4,000,000 Galaxies at z 2-7: Galaxy-AGN Transition, Star Formation Efficiency, and Implication for Evolution at $z \gtrsim 10$* , *ApJS* **259** (2022) 20 [[2108.01090](#)].
- [8] C.T. Donnan, D.J. McLeod, J.S. Dunlop, R.J. McLure, A.C. Carnall, R. Begley et al., *The evolution of the galaxy UV luminosity function at redshifts $z = 8 - 15$ from deep JWST and ground-based near-infrared imaging*, *MNRAS* **518** (2023) 6011 [[2207.12356](#)].
- [9] Y. Harikane, M. Ouchi, M. Oguri, Y. Ono, K. Nakajima, Y. Isobe et al., *A Comprehensive Study of Galaxies at z 9-16 Found in the Early JWST Data: Ultraviolet Luminosity Functions and Cosmic Star Formation History at the Pre-reionization Epoch*, *ApJS* **265** (2023) 5 [[2208.01612](#)].
- [10] R. Bouwens, G. Illingworth, P. Oesch, M. Stefanon, R. Naidu, I. van Leeuwen et al., *UV luminosity density results at $z \gtrsim 8$ from the first JWST/NIRCam fields: limitations of early data sets and the need for spectroscopy*, *MNRAS* **523** (2023) 1009 [[2212.06683](#)].
- [11] D.J. McLeod, C.T. Donnan, R.J. McLure, J.S. Dunlop, D. Magee, R. Begley et al., *The galaxy UV luminosity function at $z \simeq 11$ from a suite of public JWST ERS, ERO, and Cycle-1 programs*, *MNRAS* **527** (2024) 5004 [[2304.14469](#)].
- [12] C.T. Donnan, R.J. McLure, J.S. Dunlop, D.J. McLeod, D. Magee, K.Z. Arellano-Córdova et al., *JWST PRIMER: a new multifield determination of the evolving galaxy UV luminosity function at redshifts $z = 9 - 15$* , *MNRAS* **533** (2024) 3222 [[2403.03171](#)].
- [13] L. Whitler, D.P. Stark, M.W. Topping, B. Robertson, M. Rieke, K.N. Hainline et al., *The zrsim9 galaxy UV luminosity function from the JWST Advanced Deep Extragalactic Survey: insights into early galaxy evolution and reionization*, *arXiv e-prints* (2025) arXiv:2501.00984 [[2501.00984](#)].
- [14] M. Trenti, M. Stiavelli, R.J. Bouwens, P. Oesch, J.M. Shull, G.D. Illingworth et al., *The Galaxy Luminosity Function During the Reionization Epoch*, *ApJ* **714** (2010) L202 [[1004.0384](#)].

- [15] S. Tacchella, M. Trenti and C.M. Carollo, *A Physical Model for the $0 < z < 8$ Redshift Evolution of the Galaxy Ultraviolet Luminosity and Stellar Mass Functions*, *ApJ* **768** (2013) L37 [1211.2825].
- [16] P. Dayal, A. Ferrara, J.S. Dunlop and F. Pacucci, *Essential physics of early galaxy formation*, *MNRAS* **445** (2014) 2545 [1405.4862].
- [17] C.A. Mason, M. Trenti and T. Treu, *The Galaxy UV Luminosity Function before the Epoch of Reionization*, *ApJ* **813** (2015) 21 [1508.01204].
- [18] G. Sun and S.R. Furlanetto, *Constraints on the star formation efficiency of galaxies during the epoch of reionization*, *MNRAS* **460** (2016) 417 [1512.06219].
- [19] S. Tacchella, S. Bose, C. Conroy, D.J. Eisenstein and B.D. Johnson, *A Redshift-independent Efficiency Model: Star Formation and Stellar Masses in Dark Matter Halos at $z \gtrsim 4$* , *ApJ* **868** (2018) 92 [1806.03299].
- [20] J. Park, A. Mesinger, B. Greig and N. Gillet, *Inferring the astrophysics of reionization and cosmic dawn from galaxy luminosity functions and the 21-cm signal*, *MNRAS* **484** (2019) 933 [1809.08995].
- [21] A. Ferrara, A. Pallottini and P. Dayal, *On the stunning abundance of super-early, luminous galaxies revealed by JWST*, *MNRAS* **522** (2023) 3986 [2208.00720].
- [22] Y.-Y. Wang, L. Lei, S.-P. Tang, G.-W. Yuan and Y.-Z. Fan, *Digging into the Ultraviolet Luminosity Functions of Galaxies at High Redshifts: Galaxies Evolution, Reionization, and Cosmological Parameters*, *ApJ* **975** (2024) 285 [2405.09350].
- [23] K. Ren, M. Trenti and S.J. Mutch, *The Cosmic Web around the Brightest Galaxies during the Epoch of Reionization*, *ApJ* **856** (2018) 81 [1802.06802].
- [24] K. Ren, M. Trenti and C.A. Mason, *The Brightest Galaxies at Cosmic Dawn from Scatter in the Galaxy Luminosity versus Halo Mass Relation*, *ApJ* **878** (2019) 114 [1905.04848].
- [25] J.B. Muñoz, J. Mirocha, S. Furlanetto and N. Sabti, *Breaking degeneracies in the first galaxies with clustering*, *MNRAS* **526** (2023) L47 [2306.09403].
- [26] J. Mirocha and S.R. Furlanetto, *Balancing the efficiency and stochasticity of star formation with dust extinction in $z > 10$ galaxies observed by JWST*, *MNRAS* **519** (2023) 843 [2208.12826].
- [27] V. Gelli, C. Mason and C.C. Hayward, *The Impact of Mass-dependent Stochasticity at Cosmic Dawn*, *ApJ* **975** (2024) 192 [2405.13108].
- [28] K.-S. Lee, M. Giavalisco, C. Conroy, R.H. Wechsler, H.C. Ferguson, R.S. Somerville et al., *Mapping the Dark Matter from UV Light at High Redshift: An Empirical Approach to Understand Galaxy Statistics*, *ApJ* **695** (2009) 368 [0808.1727].
- [29] L.H. Weinberger, M.G. Haehnelt and G. Kulkarni, *Modelling the observed luminosity function and clustering evolution of Ly α emitters: growing evidence for late reionization*, *MNRAS* **485** (2019) 1350 [1902.05077].
- [30] J. Mirocha, *Prospects for distinguishing galaxy evolution models with surveys at redshifts $z \gtrsim 4$* , *MNRAS* **499** (2020) 4534 [2008.04322].
- [31] G. Sun, J.B. Muñoz, J. Mirocha and C.-A. Faucher-Giguère, *Constraining bursty star formation histories with galaxy UV and H α luminosity functions and clustering*, *arXiv e-prints* (2024) arXiv:2410.21409 [2410.21409].
- [32] H.J. Mo and S.D.M. White, *An analytic model for the spatial clustering of dark matter haloes*, *MNRAS* **282** (1996) 347 [astro-ph/9512127].
- [33] R.K. Sheth and G. Tormen, *Large-scale bias and the peak background split*, *MNRAS* **308** (1999) 119 [astro-ph/9901122].

- [34] A. Jenkins, C.S. Frenk, S.D.M. White, J.M. Colberg, S. Cole, A.E. Evrard et al., *The mass function of dark matter haloes*, **MNRAS** **321** (2001) 372 [[astro-ph/0005260](#)].
- [35] J.L. Tinker, B.E. Robertson, A.V. Kravtsov, A. Klypin, M.S. Warren, G. Yepes et al., *The Large-scale Bias of Dark Matter Halos: Numerical Calibration and Model Tests*, **ApJ** **724** (2010) 878 [[1001.3162](#)].
- [36] J. Park, H.-S. Kim, J.S.B. Wyithe, C.G. Lacey, C.M. Baugh, R.L. Barone-Nugent et al., *The clustering and halo occupation distribution of Lyman-break galaxies at $z \sim 4$* , **MNRAS** **461** (2016) 176 [[1511.01983](#)].
- [37] P.W. Hatfield, R.A.A. Bowler, M.J. Jarvis and C.L. Hale, *The environment and host haloes of the brightest $z \sim 6$ Lyman-break galaxies*, **MNRAS** **477** (2018) 3760 [[1702.03309](#)].
- [38] Y. Harikane, M. Ouchi, Y. Ono, S. More, S. Saito, Y.-T. Lin et al., *Evolution of Stellar-to-Halo Mass Ratio at $z = 0 - 7$ Identified by Clustering Analysis with the Hubble Legacy Imaging and Early Subaru/Hyper Suprime-Cam Survey Data*, **ApJ** **821** (2016) 123 [[1511.07873](#)].
- [39] C. Jose, K. Subramanian, R. Srianand and S. Samui, *Spatial clustering of high-redshift Lyman-break galaxies*, **MNRAS** **429** (2013) 2333 [[1208.2097](#)].
- [40] R. Bielby, M.D. Hill, T. Shanks, N.H.M. Crighton, L. Infante, C.G. Bornancini et al., *The VLT LBG Redshift Survey - III. The clustering and dynamics of Lyman-break galaxies at $z \sim 3$* , **MNRAS** **430** (2013) 425 [[1204.3635](#)].
- [41] R.L. Barone-Nugent, M. Trenti, J.S.B. Wyithe, R.J. Bouwens, P.A. Oesch, G.D. Illingworth et al., *Measurement of Galaxy Clustering at $z \sim 7.2$ and the Evolution of Galaxy Bias from $3.8 < z < 8$ in the XDF, GOODS-S, and GOODS-N*, **ApJ** **793** (2014) 17 [[1407.7316](#)].
- [42] Y. Qiu, J.S.B. Wyithe, P.A. Oesch, S.J. Mutch, Y. Qin, I. Labbé et al., *Dependence of galaxy clustering on UV luminosity and stellar mass at $z \sim 4-7$* , **MNRAS** **481** (2018) 4885 [[1809.10161](#)].
- [43] N. Dalmaso, M. Trenti and N. Leethochawalit, *Galaxy clustering measurements out to redshift $z \sim 8$ from Hubble Legacy Fields*, **MNRAS** **528** (2024) 898 [[2312.12329](#)].
- [44] N. Dalmaso, N. Leethochawalit, M. Trenti and K. Boyett, *Galaxy clustering at cosmic dawn from JWST/NIRCam observations to redshift $z < 11$* , **MNRAS** **533** (2024) 2391 [[2402.18052](#)].
- [45] A. Dekel, K.S. Sarkar, Y. Birnboim, N. Mandelker and Z. Li, *Efficient Formation of Massive Galaxies at Cosmic Dawn by Feedback-Free Starbursts*, *arXiv e-prints* (2023) [arXiv:2303.04827](#) [[2303.04827](#)].
- [46] A. Renzini, *A transient overcooling in the early Universe? Clues from globular clusters formation*, **MNRAS** **525** (2023) L117 [[2305.14476](#)].
- [47] X. Shen, M. Vogelsberger, M. Boylan-Kolchin, S. Tacchella and R. Kannan, *The impact of UV variability on the abundance of bright galaxies at $z \geq 9$* , *arXiv e-prints* (2023) [arXiv:2305.05679](#) [[2305.05679](#)].
- [48] A. Pallottini and A. Ferrara, *Stochastic star formation in early galaxies: JWST implications*, *arXiv e-prints* (2023) [arXiv:2307.03219](#) [[2307.03219](#)].
- [49] K. Inayoshi, Y. Harikane, A.K. Inoue, W. Li and L.C. Ho, *A Lower Bound of Star Formation Activity in Ultra-high-redshift Galaxies Detected with JWST: Implications for Stellar Populations and Radiation Sources*, **ApJ** **938** (2022) L10 [[2208.06872](#)].
- [50] A. Chakraborty and T.R. Choudhury, *Modelling the star-formation activity and ionizing properties of high-redshift galaxies*, **J. Cosmology Astropart. Phys.** **2024** (2024) 078 [[2404.02879](#)].
- [51] A. Hutter, E.R. Cueto, P. Dayal, S. Gottlöber, M. Trebitsch and G. Yepes, *Astraeus X:*

- Indications of a top-heavy initial mass function in highly star-forming galaxies from JWST observations at $z \gtrsim 10$, arXiv e-prints (2024) arXiv:2410.00730 [2410.00730].*
- [52] Planck Collaboration, P.A.R. Ade, N. Aghanim, C. Armitage-Caplan, M. Arnaud, M. Ashdown et al., *Planck 2013 results. XVI. Cosmological parameters*, *A&A* **571** (2014) A16 [1303.5076].
 - [53] J.B. Oke, *Absolute Spectral Energy Distributions for White Dwarfs*, *ApJS* **27** (1974) 21.
 - [54] J.B. Oke and J.E. Gunn, *Secondary standard stars for absolute spectrophotometry.*, *ApJ* **266** (1983) 713.
 - [55] P. Dayal, T.R. Choudhury, V. Bromm and F. Pacucci, *Reionization and Galaxy Formation in Warm Dark Matter Cosmologies*, *ApJ* **836** (2017) 16 [1501.02823].
 - [56] T.R. Choudhury and P. Dayal, *Probing the fluctuating ultraviolet background using the Hubble Frontier Fields*, *MNRAS* **482** (2019) L19 [1809.01798].
 - [57] C. Leitherer, D. Schaerer, J.D. Goldader, R.M.G. Delgado, C. Robert, D.F. Kune et al., *Starburst99: Synthesis Models for Galaxies with Active Star Formation*, *ApJS* **123** (1999) 3 [astro-ph/9902334].
 - [58] Planck Collaboration, N. Aghanim, Y. Akrami, M. Ashdown, J. Aumont, C. Baccigalupi et al., *Planck 2018 results. VI. Cosmological parameters*, *A&A* **641** (2020) A6 [1807.06209].
 - [59] R.J. Bouwens, P.A. Oesch, M. Stefanon, G. Illingworth, I. Labbé, N. Reddy et al., *New Determinations of the UV Luminosity Functions from $z = 9$ to 2 Show a Remarkable Consistency with Halo Growth and a Constant Star Formation Efficiency*, *AJ* **162** (2021) 47 [2102.07775].
 - [60] V. Mauerhofer and P. Dayal, *The dust enrichment of early galaxies in the JWST and ALMA era*, *MNRAS* **526** (2023) 2196 [2305.01681].
 - [61] J. Torrado and A. Lewis, *Cobaya: code for Bayesian analysis of hierarchical physical models*, *J. Cosmology Astropart. Phys.* **2021** (2021) 057 [2005.05290].
 - [62] A. Weibel, P.A. Oesch, L. Barrufet, R. Gottumukkala, R.S. Ellis, P. Santini et al., *Galaxy build-up in the first 1.5 Gyr of cosmic history: insights from the stellar mass function at $z = 4-9$ from JWST NIRCам observations*, *MNRAS* **533** (2024) 1808 [2403.08872].